

# Nucleosome-like, Single-stranded DNA (ssDNA)-Histone Octamer Complexes and the Implication for DNA Double Strand Break Repair\*

Received for publication, January 12, 2017, and in revised form, February 13, 2017. Published, JBC Papers in Press, February 15, 2017, DOI 10.1074/jbc.M117.776369

Nicholas L. Adkins<sup>‡</sup>, Sarah G. Swygert<sup>‡</sup>, Parminder Kaur<sup>§¶</sup>, Hengyao Niu<sup>||</sup>, Sergei A. Grigoryev<sup>\*\*</sup>, Patrick Sung<sup>||</sup>, Hong Wang<sup>§¶</sup>, and Craig L. Peterson<sup>‡1</sup>

From the <sup>‡</sup>Program in Molecular Medicine, University of Massachusetts Medical School, Worcester, Massachusetts 01605, the <sup>§</sup>Department of Physics, <sup>¶</sup>Center for Human Health and the Environment, North Carolina State University, Raleigh, North Carolina 27695, the <sup>||</sup>Department Molecular Biophysics and Biochemistry, Yale University School of Medicine, New Haven, Connecticut 06520, and the <sup>\*\*</sup>Department of Biochemistry and Molecular Biology, Pennsylvania State University College of Medicine, Hershey, Pennsylvania 17033

Edited by John M. Denu

Repair of DNA double strand breaks (DSBs) is key for maintenance of genome integrity. When DSBs are repaired by homologous recombination, DNA ends can undergo extensive processing, producing long stretches of single-stranded DNA (ssDNA). *In vivo*, DSB processing occurs in the context of chromatin, and studies indicate that histones may remain associated with processed DSBs. Here we demonstrate that histones are not evicted from ssDNA after *in vitro* chromatin resection. In addition, we reconstitute histone-ssDNA complexes (termed ssNucs) with ssDNA and recombinant histones and analyze these particles by a combination of native gel electrophoresis, sedimentation velocity, electron microscopy, and a recently developed electrostatic force microscopy technique, DREEM (dual-resonance frequency-enhanced electrostatic force microscopy). The reconstituted ssNucs are homogenous and relatively stable, and DREEM reveals ssDNA wrapping around histones. We also find that histone octamers are easily transferred *in trans* from ssNucs to either double-stranded DNA or ssDNA. Furthermore, the Fun30 remodeling enzyme, which has been implicated in DNA repair, binds ssNucs preferentially over nucleosomes, and ssNucs are effective at activating Fun30 ATPase activity. Our results indicate that ssNucs may be a hallmark of processes that generate ssDNA, and that posttranslational modification of ssNucs may generate novel signaling platforms involved in genome stability.

The repair of DNA double strand breaks (DSBs) is critical for maintaining genome integrity, as improper repair can result in the loss, duplication, or translocation of genetic information

\* This work was supported, in whole or in part, by National Institutes of Health Grants RO1 GM054096 (to C. L. P.), RO1 GM107559 (to H. W.), and F32 GM096701 (to N. L. A.) from the NIGMS, RO1 ES007061 (to H. N. and P. S.) from NIEHS, Grant P30 ES025128 to the Center for Human Health and the Environment (CHHE), and National Science Foundation Grant 1516999 (to S. A. G.). The authors declare that they have no conflicts of interest with the contents of this article. The content is solely the responsibility of the authors and does not necessarily represent the official views of the National Institutes of Health.

<sup>1</sup> To whom correspondence should be addressed: 373 Plantation St., Biotech 2, Ste. 210, Worcester, MA 01605. Tel.: 508-856-5858; E-mail: craig.peterson@umassmed.edu.

leading to numerous diseases (1–3). There are two main pathways for DNA DSB repair: error-prone, non-homologous end-joining and relatively error-free, homologous recombination (HR)<sup>2</sup> (4). During HR, the DNA ends are resected, resulting in long 3' single-stranded DNA (ssDNA) "tails," which serve as substrates for subsequent interactions with the ssDNA-binding protein, RPA, and the Rad51 DNA recombinase. In budding yeast, genetic and biochemical studies have identified two redundant pathways for DNA end resection during HR, characterized by either the Sgs1-Dna2 or Exo1 enzymes (5–7). *In vitro* studies have shown that efficient resection by the yeast Sgs1-Dna2 pathway requires a host of additional proteins, including the Mre11-Rad50-Xrs2 complex, RPA, and the Top3-Rmi1 complex (5). In contrast, Exo1 is sufficient to process dsDNA ends *in vitro* (5). Members of the budding yeast resection machinery are conserved among eukaryotes, and defects in the human homologs of Sgs1 (BLM, WRN, RECQ4) have been linked to cancer predisposition and premature aging (8).

Not only do repair enzymes carry out the multitude of enzymatic steps required for restoring DNA, but they must also contend with the inherent barrier posed by DNA packaging into chromatin. Indeed, a number of chromatin remodeling enzymes and histone posttranslational modifications are recruited to DSB chromatin and play key roles in DNA damage repair and signaling (9–15). *In vivo*, chromatin immunoprecipitation (ChIP) studies confirm that at least one nucleosome is removed immediately adjacent to a DSB, and this localized nucleosome eviction is thought to be key for efficient DSB repair (15). In cases where a DSB fails to be repaired and persists, the resection machinery processes many kilobases of DNA, but in this case the histone levels do not decrease dramatically in these regions (10, 11, 13, 16, 17). Importantly, the resection process is quite efficient, with >90% of the DSB ends processed at least 3 kilobases by 4 h of DSB formation (10, 18).

<sup>2</sup> The abbreviations used are: HR, homologous recombination; 2DSA/GA-MC, two-dimensional spectrum analysis, genetic algorithm, and Monte Carlo modeling; DREEM, dual-resonance frequency-enhanced electrostatic force microscopy; nt, nucleotide(s); TBE, Tris/borate/EDTA; Tricine, N-[2-hydroxy-1,1-bis(hydroxymethyl)ethyl]glycine; APTES, (3-aminopropyl)triethoxysilane; AFM, atomic force microscopy.

## Characterization of ssDNA-Histone Complexes

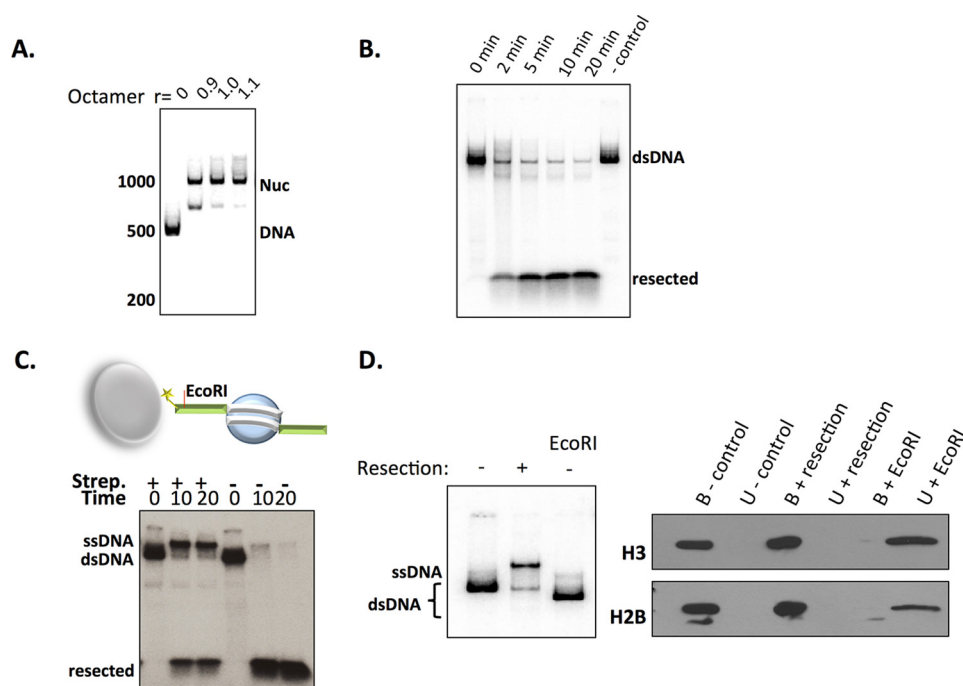


**FIGURE 1. Histone fate after *in vitro* chromatin resection by the Sgs1-Dna2 pathway.** *A*, native PAGE of a 500-bp DNA fragment harboring a central, 601-positioning sequence reconstituted into mononucleosomes by salt step dialysis at different ratios ( $r$ ) of histone octamers to DNA. Note that the minor nucleosome species is likely to represent a nucleosome assembled on the DNA end. *B* and *C*, chromatin resection time course with 3'-radiolabeled chromatin and reactions that contain Mre11-Rad50-Xrs2, Sgs1, Top3-Rmi complex, Dna2, and RPA. *C*, addition of streptavidin-coated magnetic beads inhibit chromatin resection on one strand. Note the appearance of slower migrating ssDNA. *D*, analysis of DNA and protein content following magnetic DNA pulldown after chromatin resection. *Left panel*, radiolabel analysis of DNA before (–) and after (+) resection. One sample was also treated with EcoRI prior to resection and the released DNA was analyzed. *Right panel*, histone immunoblotting of bead bound (B) and unbound (U) fractions before and after chromatin resection.

Thus, high levels of histones at processed DSBs cannot be explained by a large proportion of unprocessed DSBs.

Here we test the fate of histones after chromatin resection *in vitro*, and we characterize the properties of reconstituted, single-stranded nucleosome-like particles. We find that after resection by Sgs1-Dna2, histones are not evicted from chromatin templates, but rather remain associated with ssDNA. We also report that recombinant histone octamers can assemble on ssDNA by salt-dialysis reconstitution, creating a structure that resembles double-stranded nucleosomes. These single-stranded histone complexes, which we term ssNucs, display structural features similar to canonical nucleosomes with ssDNA wrapping around histone proteins, as shown in DREEM imaging. However, the ssNucs are inherently more dynamic, spontaneously transferring histone octamers *in trans* to ssDNA or dsDNA. We also show that the RSC and Fun30 chromatin remodeling enzymes can bind ssNucs, that these interactions activate their ATPase activity, and that Fun30 demonstrates a strong preference for ssNucs compared with canonical nucleosomes. Our results support the view that ssNucs are a hallmark of DSB chromatin that has been processed for HR, and we suggest that these structures may present novel opportunities for histone posttranslational modifications to contribute to the cellular response to DNA damage.

### Results

**Histones Remain Associated with Single-stranded DNA after *in Vitro* DNA Resection**—Previously, we reported that nucleosomes are not a barrier for DNA resection by the Sgs1-Dna2 machinery if sufficient free DNA is located adjacent to a posi-

tioned nucleosome (19). To investigate the fate of histones after DNA processing by Sgs1-Dna2, we assessed histone association with ssDNA during resection of nucleosomes immobilized on magnetic beads. Recombinant histones were used to reconstitute a mononucleosome on a 500-bp DNA fragment that harbors a center-positioned, 601-nucleosome positioning sequence (Fig. 1A). The DNA was labeled with  $^{32}\text{P}$  on the 3' end and with a biotinylated nucleotide on the 5' end (see schematic in Fig. 1C). After addition of the Sgs1-Dna2 resection machinery, DNA within the chromatin substrate was rapidly processed, indicated by the appearance of small fragments of resected DNA over time (Fig. 1B; see also Ref. 19). The labeled mononucleosomes were then bound to streptavidin magnetic beads, and unbound complexes were removed by magnetic capture and washing. The immobilization of nucleosomes blocked resection from one end, resulting in accumulation of a ssDNA product (Fig. 1C). Note that resection proceeded to very small, limited digestion products in the presence or absence of streptavidin beads, indicating that the reaction went to completion and that no significant dsDNA remained. To determine the fate of histones after DNA resection, the bead-bound and free fractions were analyzed by native PAGE and Western blot analyses (Fig. 1D). Strikingly, histone H3 and H2B remained bound to the beads (Fig. 1D, *right panel*), even though nearly all the bead-bound DNA was single-stranded (Fig. 1D, *left panel*). Note that histones could be efficiently removed from the beads by EcoRI digestion prior to resection, consistent with proper nucleosome assembly (Fig. 1D, *right panel*). These data are consistent with retention of histones on ssDNA following Sgs1-Dna2-dependent chromatin resection.

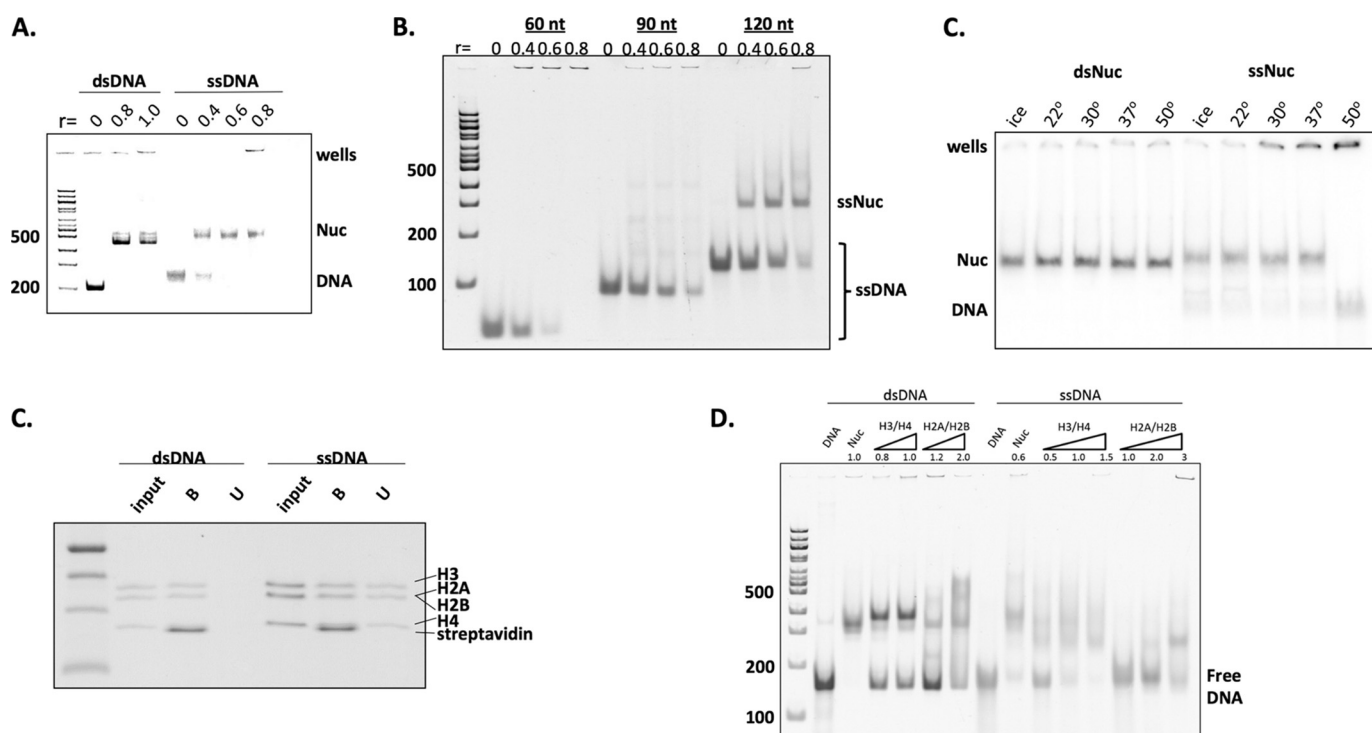
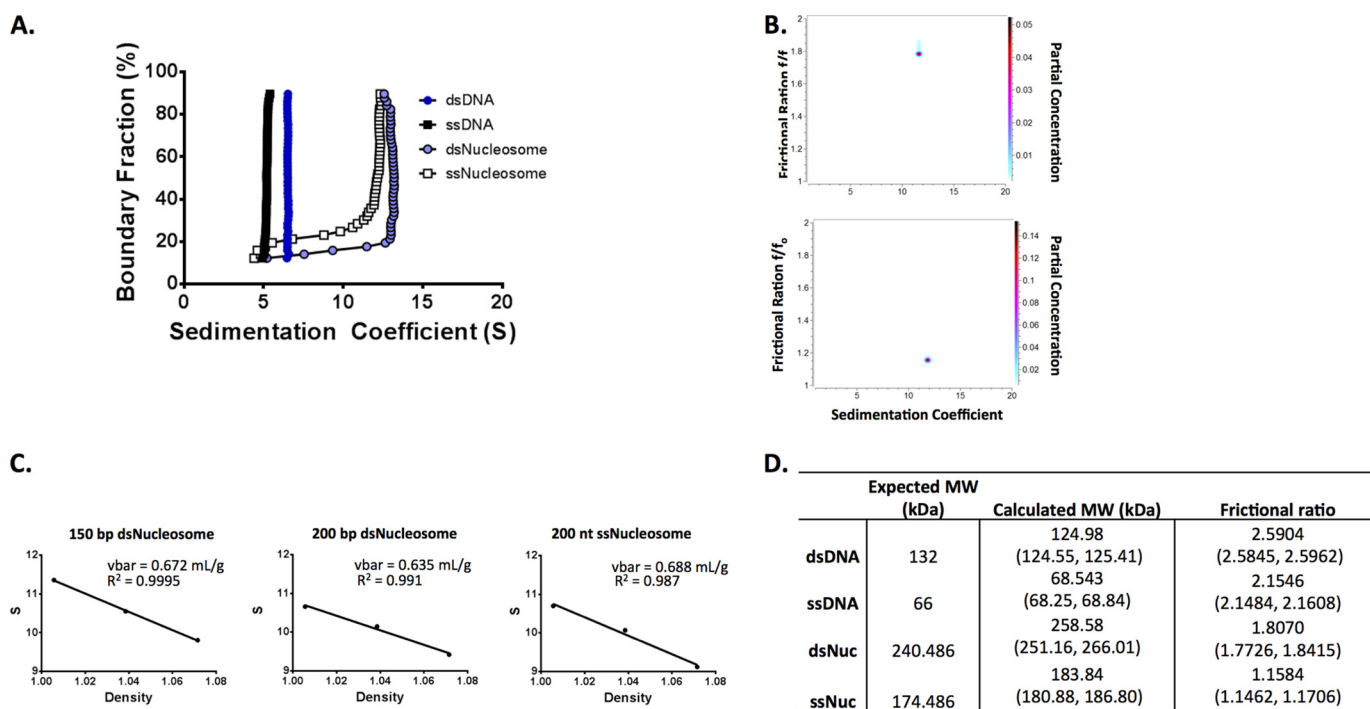


FIGURE 2. **Biochemical characterization of reconstituted mononucleosomes.** *A*, native PAGE of the indicated nucleic acid with increasing histone ratios ( $r$ ) after reconstitution by salt step dialysis. Note that ssDNA stains less intensely with ethidium bromide. *B*, 4% native PAGE of ssDNA-histone octamer reconstitutions, using radiolabeled DNA fragments of varying length.  $r$ , histone octamer:DNA molar ratio. *C*, the stability of double-stranded and single-stranded nucleosomes after a 1-h incubation at the indicated range of temperatures, analyzed by separation on a 4% native PAGE. *D*, 200-nt ssDNA or 200-bp dsDNA chromatin reconstitutions were immobilized on streptavidin-coated magnetic beads, and histone content was analyzed after magnetic pulldown by SDS-PAGE. *E*, the indicated histone complexes were used in chromatin reconstitution reactions with 150-bp or 150-nt DNA fragments. Reconstitutions were analyzed by 4% native PAGE.

*ssDNA-Histone Octamer Complexes Can Be Reconstituted in Vitro*—To investigate if histones can assemble nucleosome-like particles on ssDNA, salt dialysis was used to reconstitute nucleosomes on 200-base pair (bp) dsDNA and 200-nucleotide (nt) ssDNA templates with recombinant histone octamers. Surprisingly, assembly of ssDNA-histone complexes was efficient, forming at similar histone-DNA ratios as canonical nucleosomes, with little evidence of nonspecific aggregates (Fig. 2*A*; note that ssDNA stains less intensely with ethidium bromide). Furthermore, ssDNA complexes migrated with similar mobility to dsDNA nucleosomes on native PAGE (Fig. 2*A*). ssDNA-histone particles could be assembled on fragments as small as 120 nt, but little assembly was observed for 60- or 90-nt templates (Fig. 2*B*). The ssDNA-histone particles were stable even after prolonged incubation at 37 °C, but they were disrupted at 50 °C, whereas canonical nucleosomes remained stable (Fig. 2*C*). To characterize the composition of single-stranded histone complexes, we reconstituted ssDNA and dsDNA complexes with biotin-labeled DNA, and histone stoichiometry was analyzed following magnetic bead capture by SDS-PAGE (Fig. 2*D*). Strikingly, ssDNA-histone complexes contain similar ratios of the four core histones as double-stranded samples (Fig. 1*D*). Additionally, native PAGE migration of single-stranded particles reconstituted with only H2A-H2B dimers or H3-H4 tetramers migrate differently than particles reconstituted with all four core histones, providing additional evidence that ssDNA-histone complexes contain histone octamers (Fig. 1*E*).

To further assess the homogeneity and stability of ssDNA-histone complexes, reconstitutions were analyzed by sedimentation velocity analytical ultracentrifugation (Fig. 3). Interestingly, the sedimentation profiles of ssDNA-histone complexes are comparable with nucleosomes, with a nearly homogeneous distribution of sedimentation coefficients of  $\sim 12$ – $13$  S (Fig. 3*A*). Recently, we have used two-dimensional spectrum analysis, genetic algorithm, and Monte Carlo modeling (2DSA/GA-MC) to fit native molecular weight and shape information to sedimentation profiles (20–22), which we applied to nucleosomes and ssDNA-histone complexes (Fig. 3*B*). This process required experimentally determining the partial specific volumes ( $\bar{v}$ ) of these molecules (Fig. 3*C*). Consistent with our previous analyses, 2DSA/GA-MC modeling yielded accurate measurements of molecular mass for dsDNA, ssDNA, and mononucleosome samples (125 kDa, 68.5 kDa, and 258.6 kDa, respectively) (Fig. 3*D*). Furthermore, this analysis predicts a native molecular mass for the ssDNA-histone complexes that is consistent with the binding of an octamer of core histones to a single molecule of ssDNA ( $\sim 184$  kDa). Strikingly, the ssDNA and dsDNA complexes have distinct, modeled frictional ratios (1.80 for mononucleosome and 1.16 for ssDNA particles; Fig. 3*D*). A frictional ratio close to 1.0 indicates particles with a spherical, symmetric shape, with higher ratios indicative of molecules that are more extended and anisotropic. Thus, these data indicate that the ssNucs are more spherical than nucleosomes. This may be due to the fact that the ssDNA that pro-

## Characterization of ssDNA-Histone Complexes



**FIGURE 3. Analysis of ssDNA-histone complexes by sedimentation velocity analyses.** *A*, van Holde Weischet analysis of analytical ultracentrifugation sedimentation profiles for 200-bp dsDNA, 200-nt ssDNA, ssNucs, and mononucleosomes. *B*, 2DSA/GA-MC modeling of samples analyzed in *A*. Note the presence of a single, major solute for both ssNucs (lower panel) and nucleosomes (upper panel). *C*, experimental determination of the  $\bar{v}$  parameter. Plots of sedimentation coefficient versus solvent density of the indicated particles sedimented in three different ratios of heavy oxygen to distilled water. Numbers in brackets represent the  $\bar{v}$  of the respective molecule as predicted by UltraScan3. *D*, native molecular weights (MW) and  $f/f_0$  ratios (frictional ratio) derived from 2DSA/GA-MC modeling. The 95% confidence intervals are shown in parentheses.

trudes from the ssDNA particle is less rigid than dsDNA, creating a more globular particle that is less subject to friction during sedimentation. Alternatively, ssDNA-histone complexes may assume an entirely distinct conformation.

To directly visualize ssDNA-histone octamer complexes, reconstitutions were analyzed using both electron microscopy (EM) and DREEM imaging (Fig. 4). Negative stain EM and AFM topography images reveal that the ssDNA-histone complexes, termed ssNucs, are similar to canonical nucleosomes (Fig. 4, *A* and *B*). In addition, nucleosomes and ssNucs display comparable heights by AFM (double strand,  $3.2 \pm 0.7$  nm; single strand,  $3.2 \pm 0.6$  nm, Fig. 4C). These values are consistent with double-stranded nucleosomes measured previously from AFM images (23, 24). DREEM imaging simultaneously collects topographic and electrostatic signals (25). To collect the topographic information, the AFM is operated in repulsive AC (intermittent contact) mode, with cantilever mechanically vibrating near its resonance frequency. To simultaneously collect the electrostatic signals, AC and DC biases are applied to a highly doped silicon cantilever with the frequency of the AC bias centered on the first overtone of the cantilever. Taking advantage of the difference in the electrostatic signals from protein and DNA molecules, DREEM reveals the path of DNA in protein-DNA complexes, as it passes around or through proteins (25–27). Proteins show a greater contrast (darker) than DNA relative to the mica surface, allowing identification of the DNA path in a protein-DNA complex. Whereas in DREEM phase images, free histone proteins display dark contrast on the mica surface (25, 26), nucleosomes reconstituted on 200-bp (Fig. 5A) and 200-nt DNAs (Fig. 5B) show brighter regions consistent with signals

from DNA seen in previous DREEM studies (25–27). These features are reproducible in multiple scans, scans at different angles, and in trace and retrace images. The orientation of the DNA paths in the respective DREEM images of nucleosomes as well as ssNucs are completely random on the APTES-treated mica surface. This indicates that the DNA signals seen in DREEM images are not due to imaging artifacts (Fig. 5, *A* and *B*). Double strand nucleosomes display the expected wrapping around the histone octamers (Fig. 5C), comparable with the previous DREEM images of nucleosomes extracted from HeLa cells, as well as nucleosomes reconstituted *in vitro* (25, 26). ssNucs display similar structural features. Importantly, in the DREEM phase images, similar to double strand nucleosomes (75%), the majority of ssNucs (88.2%) show two wraps of DNA around histone octamers (Fig. 5D). The two DNA wraps can be clearly identified from the cross-section analysis of DREEM images of ssNucs, but not from topographic AFM images (Fig. 5E). Taken together, these results indicate that histone octamers can assemble nucleosome-like structures on ssDNA templates, with ssDNA wrapping around histones with more than one turn.

*ssNuc Readily Transfer Histone Octamers to Acceptor DNAs*—Previous studies have emphasized the stability of nucleosomes, with either high heat or ATP-dependent remodeling enzymes required for most alterations to nucleosome structure, composition, and positioning. To characterize ssNuc stability, increasing amounts of dsDNA or ssDNA were incubated with ssNucs or canonical nucleosomes. Surprisingly, histone octamers on ssDNA readily transfer to both dsDNA and ssDNA in the absence of enzymes or ATP (Fig. 6A). This transfer was not

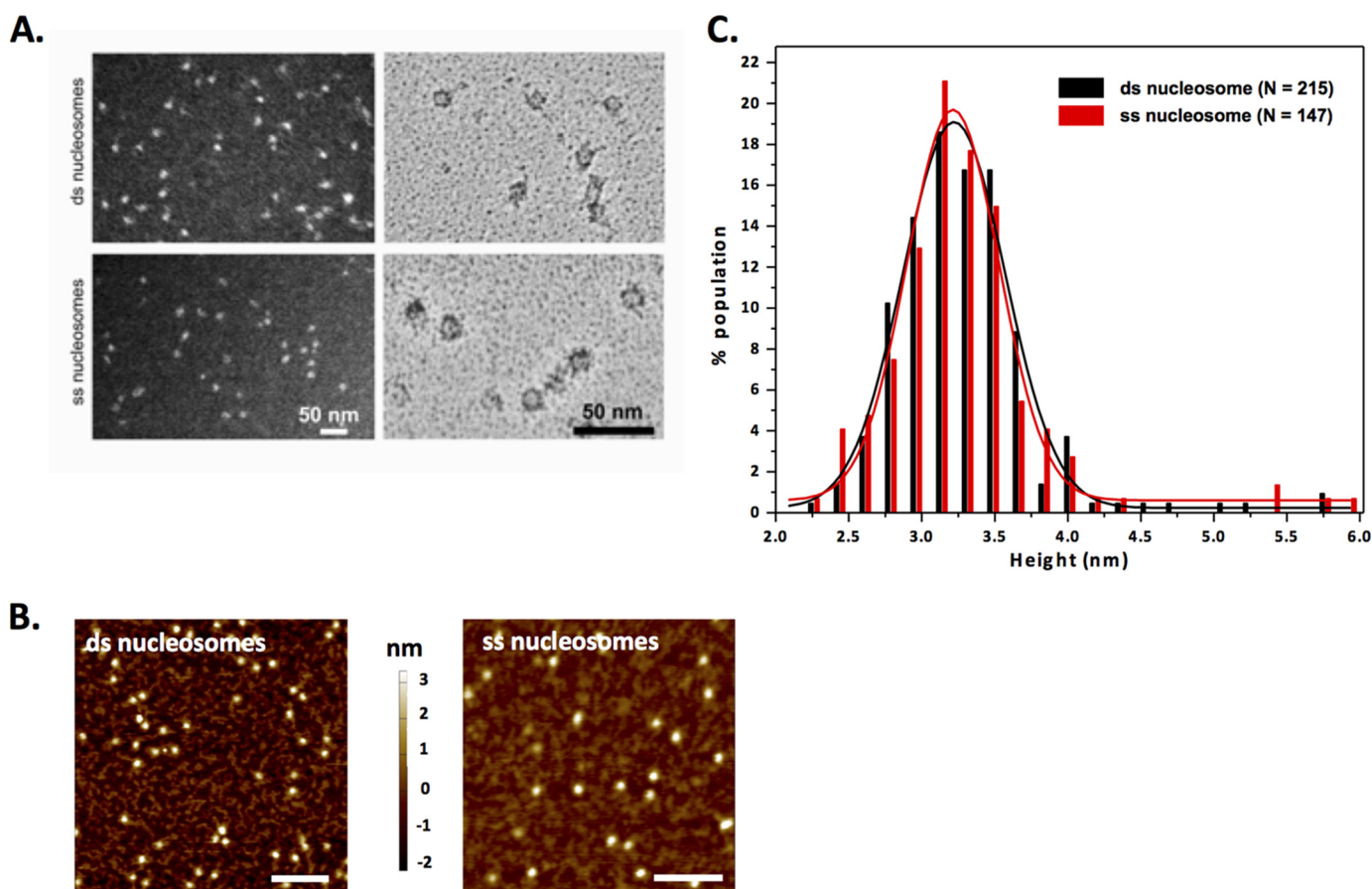


FIGURE 4. **EM and AFM imaging of ssNucs and ds nucleosomes.** *A*, electron microscopy of ds (top) and ss (bottom) nucleosomes. Samples were stained with uranyl acetate and processed for dark-field (left panels) or bright-field (right panels) imaging. *B*, AFM topographic images of ds (left) and ss (right) nucleosomes. *x-y* scale bar = 100 nm. *C*, the AFM height distributions for double and single strand nucleosomes. The solid lines show the Gaussian fit to the data. The average heights of double and single strand nucleosomes are  $3.2 \pm 0.7$  nm (S.D.) ( $n = 215$ ) and  $3.2 \pm 0.6$  nm (S.D.) ( $n = 147$ ), respectively.

observed for canonical nucleosomes. Notably, transfer does not require free DNA ends on the accepting molecule, as circular dsDNA was also a potent acceptor for histone octamers from ssNucs (Fig. 6*B*). Taken together, these data suggest that although ssNucs are stable in solution, they are highly dynamic structures in the presence of competing DNAs.

*The ATP-dependent Remodeling Enzyme Fun30 Preferentially Interacts with ssNucs*—Previous *in vivo* studies have found that many ATP-dependent chromatin remodeling enzymes are recruited to sites of DNA DSBs, although their functions during HR repair remain poorly characterized (9–11, 13, 18). Our data suggest that ssNucs may be retained on ssDNA following resection and consequently may serve as substrates for ATP-dependent chromatin remodeling complexes. Consistent with this view, recruitment of chromatin remodeling enzymes (e.g. SWI/SNF, RSC, INO80C, SWR1C, NuA4, and FUN30) to DSBs is greatly enhanced by DSB resection (11, 18). The yeast RSC and Fun30 remodeling enzymes have been implicated in the early and late stages of DSB processing, respectively (15, 18, 28, 29). Although our previous study indicated that neither RSC nor Fun30 enhances *in vitro* resection of chromatin substrates (19), it remains possible that they act on ssNucs remaining after resection. To investigate functional interactions with ssNucs, RSC and Fun30 were purified and then incubated at increasing ratios with radiolabeled nucleosomes or ssNucs, and the resulting complexes were analyzed by gel electrophoresis (Fig. 7, *A* and *B*).

RSC and Fun30 formed complexes with both ssNucs and nucleosomes, but RSC showed little preference for either substrate, whereas Fun30 displayed a greater affinity for ssNucs. Note that the Fun30-ssNuc complexes were rather diffuse, suggesting that the complex may be prone to dissociation during gel electrophoresis. The specificity of Fun30 for ssNucs was additionally corroborated by an increase in the rate of ATP hydrolysis in the presence of single-stranded substrates (Fig. 7, *C* and *D*). Strikingly, Fun30 displayed a 25-fold increase in  $K_m$  for ssDNA compared with dsDNA, and a 4-fold increase in  $K_m$  for ssNucs compared with nucleosomes. In contrast, RSC has a very similar  $K_m$  for ssDNA and dsDNA, and a 2-fold decrease in  $K_m$  for ssNucs. Taken together, these results demonstrate that Fun30 prefers ssDNA as a substrate, and that ssNucs may promote Fun30-mediated activity during DNA repair.

## Discussion

The structural similarities between single-stranded, nucleosome-like particles (ssNucs) and double-stranded nucleosomes are striking, with similar conformations and histone stoichiometry as determined by EMSA, EM, DREEM, and analytical ultracentrifugation. In contrast to canonical nucleosomes, ssNucs are highly dynamic, as histone octamers were readily trans-

## Characterization of ssDNA-Histone Complexes

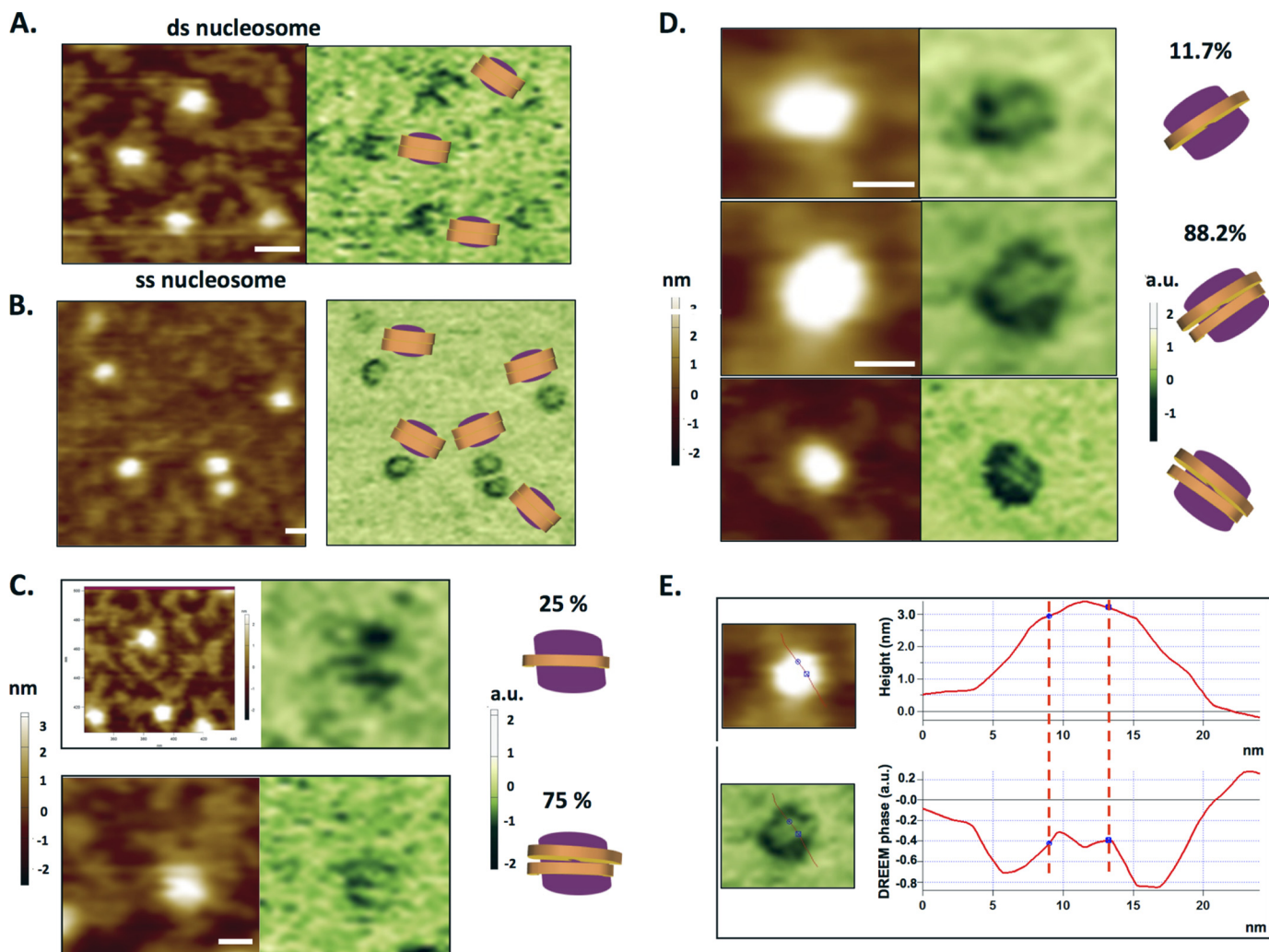


**FIGURE 5. DREEM phase images of nucleosomes and ssNucs.** *A* and *B*, AFM topography (*left panels*) and DREEM phase images (*right panels*) of double (*A*) and single (*B*) strand nucleosomes. The models depict the orientation of DNA based on DREEM images. *C* and *D*, AFM topography (*left panels*) and DREEM phase images (*right panels*) of double strand (*C*) and single strand (*D*) nucleosomes showing one strand (*top panels*) or two strands of DNA (*bottom panels*). *x-y* scale bar = 10 nm. The *panels on the right* show the models based on DREEM phase images and percentages of nucleosomes with one strand or two strands of DNA revealed in DREEM images. The total number of nucleosomes analyzed are 44 and 222 for double and single strand nucleosomes, respectively. *E*, cross-section analysis of one of the single strand nucleosome shown in *D*.

ferred to other DNA molecules in *trans*. Furthermore, ssNucs were formed on DNA lengths as small as 90 nt, but particle stability was greatly enhanced by increasing the length of ssDNA to 200 nt. Our studies are consistent with several older studies where histones were reconstituted on single strand phage DNAs, poly(dT), or denatured genomic DNA fragments (30–32). In these previous cases, nuclease protection studies also suggested that histones could associate with ~100 nt of ssDNA (30, 31). We found that the assembly of ssDNA-histone complexes was efficient at nearly the same histone-DNA ratios as required for canonical nucleosome assembly, and sedimentation velocity studies support the view that a single strand of ssDNA wraps onto a histone octamer. Furthermore, DREEM imaging showed that ssNucs are similar to canonical nucleosomes, displaying two wraps of ssDNA on a histone octamer. Taken together, our data suggest that the reconstitution of histone octamers on ssDNA leads to particles that closely resemble canonical nucleosomes in which dsDNA is wrapped nearly two turns.

Perhaps the key question is do ssNucs form *in vivo*? The best evidence for the existence of ssNucs comes from studies of DSB

repair in yeast. Following formation of a chromosomal DSB induced by the yeast HO endonuclease, DNA ends are resected at a rate of ~4 kb per h (29), and studies from many groups have used chromatin immunoprecipitation assays to monitor histone density in chromatin that surrounds a DSB at different time points during DSB processing (10, 11, 13, 16, 17). In nearly all cases, histone levels are rapidly depleted immediately adjacent to the DSB (<500 bp), but levels decline only 2–4-fold within 1 kb of the DSB, even after ~8 kb of resection (2 h). At later time points (4–5 h), few changes in histone levels are observed from 5 to 25 kb from the DSB, even though DSB processing has proceeded for at least 16 kb. Notably, the retention of histone ChIP signals on resected DNA does not appear to be due to changes in the cross-linking efficiency of histones to ssDNA, as we find that histones cross-link with similar efficiencies to ssDNA and dsDNA *in vitro*.<sup>3</sup> Furthermore, quantitative analysis of DSB resection confirms that less than 10% of DSB

<sup>3</sup> N. L. Adkins and C. L. Peterson, unpublished results.

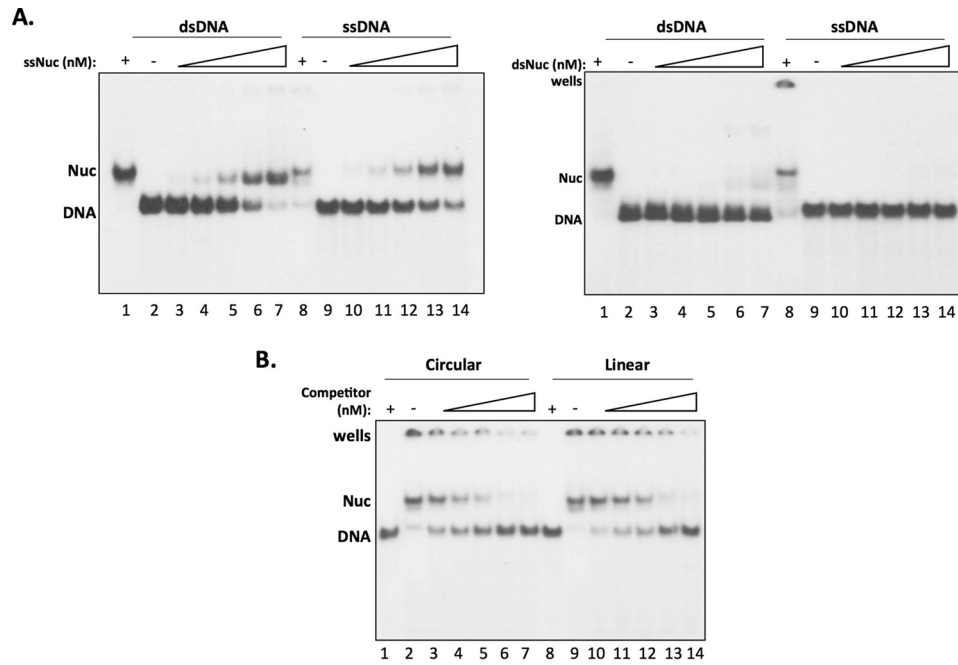


FIGURE 6. **Single strand nucleosomes transfer histone octamers between DNA strands.** *A*, native PAGE of radiolabeled naked DNA (5 nM) incubated with increasing concentrations of unlabeled, ssNucs (5, 10, 20, 50, 100 nM) (*left*) or unlabeled, nucleosomes (*right*). *Lanes 1* and *8* of each panel contains radiolabeled nucleosome or ssNuc as a marker. *B*, native PAGE of radiolabeled, single strand nucleosomes (1 nM) incubated with increasing concentrations of circular and linear naked DNA (0.2, 1, 2, 10, and 20 nM). *Lanes 1* and *8* contain radiolabeled, free nucleosome template DNA as a marker.

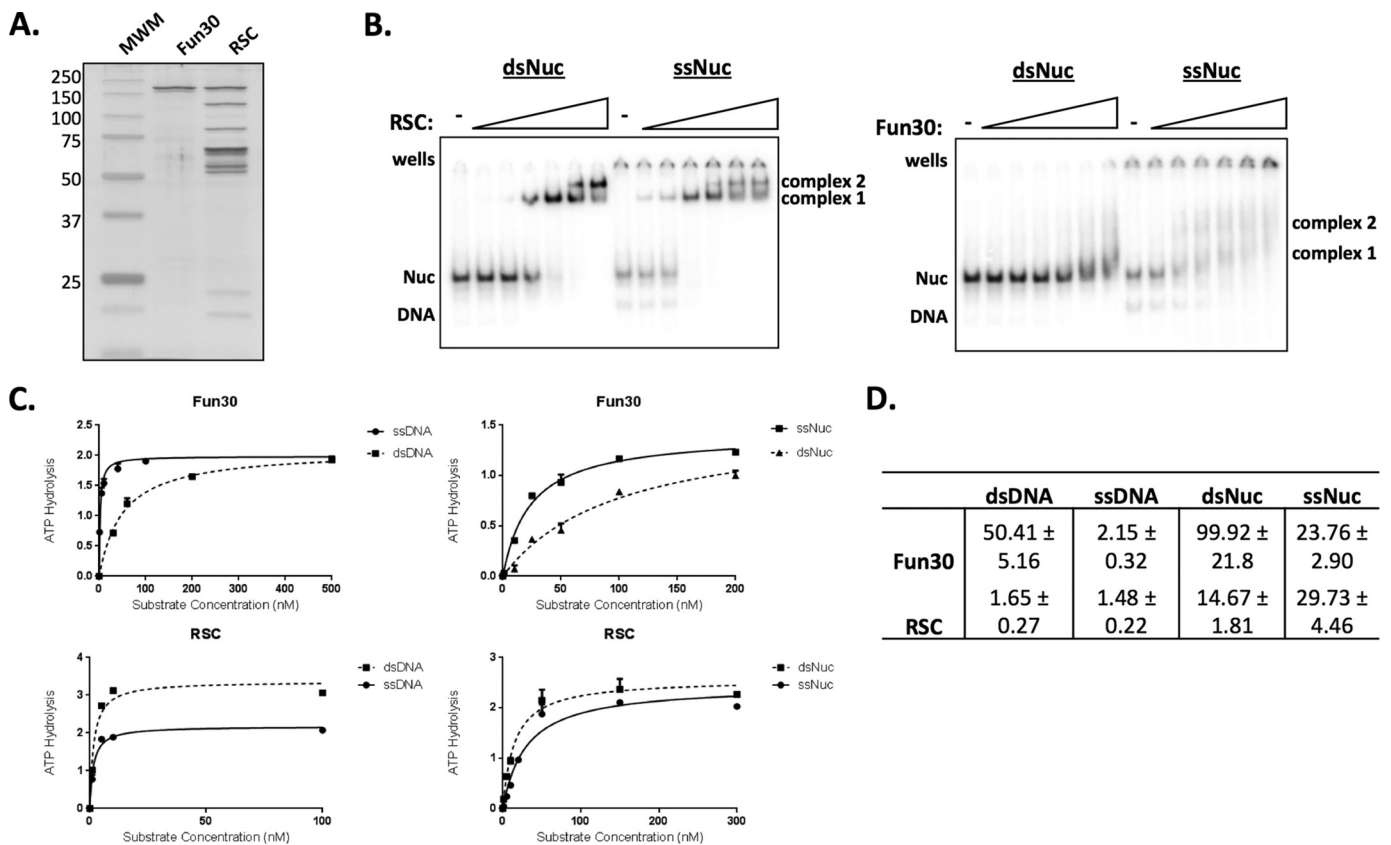


FIGURE 7. **The ATP-dependent remodeling enzyme Fun30 prefers single-stranded chromatin.** *A*, SDS-PAGE analysis of purified Fun30 and RSC enzymes. *MWM*, molecular weight marker. *B*, electrophoretic mobility shift assay of RSC (*left*) and Fun30 (*right*) binding to nucleosomes (dsNuc) or ssNucs. Michaelis-Menten kinetics (*C*) and  $K_m$  parameters (*D*) for ATPase activities of RSC and Fun30 with the indicated substrates. Units for  $K_m$  values are nM.

ends remain double stranded by 4 h after DSB formation (18). Interestingly, Osley and colleagues (10) found that inactivation of the INO80C remodeler had no effect on DSB resection, but

eliminated histone loss at DSB chromatin. This result led Osley and colleagues (10) to postulate the existence of nucleosomes remaining on ssDNA and that they might be targeted by

## Characterization of ssDNA-Histone Complexes

remodeling enzymes. These studies are consistent with the results of our *in vitro* resection assays, where histones are retained following Sgs1/Dna2-dependent resection. In this case, we envision that nucleosomes are disassembled by the helicase activity of Dna2, and that ssNucs are then reassembled on the resulting ssDNA.

If histones are retained on ssDNA, what are the possible consequences for DSB repair and the DNA damage response (DDR)? Numerous *in vivo* studies have reported that phosphorylation of histone H2A in yeast and H2A.X in mammals ( $\gamma$ H2AX) accumulates within chromatin >500 bp distal to the DSB, consistent with histones remaining associated with DNA adjacent to a processed DSB. This histone mark is established by the ataxia telangiectasia-mutated (ATM) and ataxia telangiectasia and Rad3-related (ATR) checkpoint kinases, interacts with checkpoint factors, and helps to maintain a robust checkpoint response (33). Other histone marks are also associated with DSB chromatin (e.g. histone H3-K4me, H4-K20me), and these modifications, along with their binding partners, are also likely to be associated with ssNucs. Furthermore, stretches of ssDNA between ssNucs may be bound to the single strand-binding protein, RPA, which is key for recruitment of the ATRIP checkpoint signaling complex (34). Overall, this suggests a quite different view of the DDR signaling platform adjacent to a DSB.

Recently, we reported that the recruitment of many chromatin remodeling enzymes to a DSB is stimulated by DSB processing (11). These results not only link the function of such chromatin regulators to HR, but also suggest that they may play roles involving ssNucs. Fun30 is an example of a remodeling enzyme that requires resection for recruitment to DSB chromatin (18). It promotes long range DNA resection (>10 kb), and genetic studies indicate that it promotes resection by antagonizing the Rad9 checkpoint factor (18, 28, 29). Although Fun30 does not stimulate chromatin resection *in vitro*, our current data indicates that Fun30 binds with high affinity to ssDNA, and Fun30 ATPase activity is preferentially activated by ssNucs compared with canonical nucleosomes. One intriguing possibility is that Fun30 may remodel ssNucs and that such an activity may either evict or otherwise antagonize Rad9.

If ssNucs are associated with DSB chromatin, this may lead to ramifications for the late steps of HR. First, ssNucs may play a positive role in a successful homology search, as they may occlude ssDNA that is distal to the 3' end of the invading filament, preventing formation of internal, unstable joint molecules. However, at later steps of repair, ssNucs might inhibit the strand invasion, branch migration, or strand capture steps of HR, and in these cases, their removal might provide a new target activity for chromatin remodeling enzymes. It may also be that the enhanced dynamics of ssNucs limits their ability to impede steps in the HR process. In any case, given that histones readily assemble onto ssDNA, the textbook illustration of HR in eukaryotes as a process that involves naked DNA molecules seems highly implausible.

Finally, the occurrence of ssNucs is unlikely to be unique to the DNA damage response. For instance, the stalling of a replication fork at a DNA lesion can lead to uncoupling of the replicative helicase from the DNA polymerase, leading to unwind-

ing of many kilobases of DNA (35). Like the case with the DDR, these events are likely to generate arrays of ssNucs that may not only play direct roles in the checkpoint signaling process, but may also generate impediments for a subsequent replication fork re-start event. Thus, it is likely that regulatory mechanisms have evolved to both exploit and contend with these novel protein-DNA structures.

### Experimental Procedures

**Protein Purification**—Resection proteins (Mre11-Rad50-Xrs2, Top3-Rmi1, Sgs1, Dna2, and RPA) were expressed and purified as previously described (5). Briefly, the Mre11-Rad50-Xrs2 complex was assembled from proteins individually expressed in yeast from genes subcloned into pPM231 under an inducible galactose promoter. Proteins were purified to near homogeneity by column chromatography and complex assembly was performed on ice at a 3:2:1.5 mg ratio of Mre11-Rad50-Xrs2. Top3-Rmi1 were recombinantly co-expressed from BL21 Rosetta cells and purified from extracts with a 5-ml SP-Sepharose column. Sgs1 was expressed in insect cells and purified with anti-FLAG-M2 resin (Sigma). Dna2 was expressed in yeast from pGAL10-Dna2 that contains a FLAG and HA double tag. Extracts were subsequently purified over a nickel-nitrilotriacetic acid-agarose column (Qiagen) followed by anti-FLAG-M2 (Sigma) batch purification. RPA subunits were overexpressed in yeast from plasmids under the *GAL10* promoter and then purified through columns of Affi-Gel Blue-agarose (Bio-Rad), Macroprep hydroxyapatite (Pharmacia Biotech), and a Mono Q column (GE Healthcare).

Recombinant *Xenopus laevis* histones were individually expressed, purified, and quantified by standard protocols (36). The ATP-dependent remodeling enzymes, RSC and Fun30, were purified from *Saccharomyces cerevisiae* RSC-TAP and Fun30-TAP strains as previously described for yeast SWI/SNF (37).

**DNA Substrate Generation**—Double-stranded DNA substrates were generated by PCR using the 601 pGem-3Z (CP1024) as the template. Biotinylation of the 5' end was incorporated by using biotinylated forward primers. Radiolabeling of the 3' end was performed after BsaI treatment of PCR products with Klenow (New England Biolabs) fill-in at room temperature with [ $\alpha$ - $^{32}$ P]dATP. Samples were phenol/chloroform extracted and passed through a Sephadex G-25 column. Single-stranded DNA substrates were custom ordered with PAGE purification from Integrated DNA Technologies (IDT). Radiolabeling of ssDNA was performed at 37 °C with T4 polynucleotide kinase (New England Biolabs) and [ $\gamma$ - $^{32}$ P]dATP. T4 polynucleotide kinase was heat inactivated at 65 °C for 20 min and free nucleotides were removed by a Sephadex G-25 column.

**Chromatin Reconstitution**—Histone octamers were assembled as previously described (38). Briefly, octamers were assembled with denatured histones in 7 M guanidine and refolded through dialysis against buffer containing 2.0 M NaCl. Histone octamers were subsequently purified by size exclusion chromatography (GE Superdex 200) and quantified by  $A_{276}$  with 0.45 equaling octamer mass of 1 mg/ml. Mononucleosomes were reconstituted at increasing ratios (r) of histone octamers to DNA template by standard salt step dialysis protocols. Nucleo-



some assembly was monitored by  $0.5\times$  Tris/borate/EDTA (TBE), 4% PAGE with ethidium bromide staining.

**DNA Resection Assay**—Assay was performed in 10- $\mu$ l reactions as previously described to monitor DNA resection rates with 0.5 nM DNA ends and 10 nM MRX complex, 10 nM Sgs1, 10 nM Top3-Rmi1 complex, 20 nM Dna2, and 100 nM RPA at 30 °C for 15 min (40 mM Tris-HCl, pH 7.5, 2 mM ATP, 2 mM MgCl<sub>2</sub>, 50 mM KCl, 1 mM DTT, 100  $\mu$ g/ml of BSA, and ATP-regenerating system of 20 mM creatine phosphate and 20  $\mu$ g/ml of creatine kinase). To assess DNA processing, samples were deproteinized after incubation by SDS (1%) and proteinase K (0.5 mg/ml) at 37 °C for 10 min before separation by a 1% agarose gel in  $1\times$  Tris/acetic acid/EDTA. Gels were dried and analyzed by phosphorimaging (GE Storm 820) or X-ray film exposure. Reaction volume for immunoblotting was performed at 25  $\mu$ l with  $\sim$ 100 ng of bead-bound chromatin and 8 nM MRX, 8 nM Sgs1, 8 nM Top3-Rmi1, 16 nM Dna2, and 160 nM RPA. To monitor histone occupancy after chromatin resection, mononucleosomes were preincubated with streptavidin-coated magnetic beads at room temperature for 15 min prior to addition of resection proteins. Chromatin was magnetically precipitated with streptavidin-coated beads (Dynabeads M-280 Streptavidin, Invitrogen) and beads were then washed twice with 10 mM Tris-HCl, pH 7.5, 50 mM NaCl, 0.5 mg/ml of BSA to remove unbound chromatin. After incubation with resection proteins (40 mM Tris-HCl, pH 7.5, 2 mM ATP, 2 mM MgCl<sub>2</sub>, 50 mM KCl, 1 mM DTT, 100  $\mu$ g/ml of BSA, and ATP-regenerating system of 20 mM creatine phosphate and 20  $\mu$ g/ml of creatine kinase) at 30 °C for 60 min, samples were magnetically precipitated with the supernatant removed and saved. DNA bound beads were washed twice with reaction buffer, and resuspended in  $1\times$  SDS loading dye. Bead-bound proteins and unbound supernatant proteins in  $1\times$  SDS loading dye were heat denatured at 100 °C for 5 min and separated on an 18% SDS-PAGE, then transferred to PVDF membrane. Immunoblotting was performed with standard protocols using histone H2B (Abcam) and H3 (Abcam) antibodies.

**Transmission Electron Microscopy**—Reconstituted ssDNA- and dsDNA-nucleosomes were fixed by 0.1% glutaraldehyde for 16 h at 4 °C, followed by dialysis against two changes of HEGN (10 mM Hepes, 0.25 mM EDTA, 2.5 mM NaCl) buffer for a total of 20 h. The dialyzed samples were diluted with 50 mM NaCl and samples were applied to carbon-coated and glow-discharged EM grids (T1000-Cu, Electron Microscopy Sciences), stained with 0.04% uranyl acetate with or without subsequent rinsing in ddH<sub>2</sub>O. Dark-field (for samples rinsed in ddH<sub>2</sub>O) and bright-field (for samples not rinsed) EM imaging was conducted at 120 kV using JEM-1400 electron microscope (JEOL USA, Peabody, MA) and images were recorded with a SC1000 ORIUS 11 megapixel CCD camera (Gatan Inc., Warrendale, PA). Tiff images were processed with ImageJ FFT bandpass filter.

**AFM Sample Preparation**—Reconstituted ssDNA- and dsDNA-histone complexes (200 and 150 nt) were diluted in  $1\times$  PBS buffer and deposited onto freshly prepared APTES mica surface as described previously (22). After incubating for 30 min, the incubated samples were first washed with the PBS

buffer followed by DI water and further dried under a stream of nitrogen gas.

**AFM and DREEM Imaging**—All AFM images were collected using a MFP-3D-Bio AFM (Asylum Research) and the samples were scanned using highly doped Pointprobe® PPP-FMR probes (Nanosensors, force constant:  $\sim$ 2.8 N/m, resonant frequency:  $\sim$ 70 kHz). All topographic images were captured at a scan rate of 1–2 Hz and a resolution of 512  $\times$  512 pixels.

For DREEM imaging, as described previously (25–27), AFM cantilevers were scraped with tweezers to remove the oxidized layer and the top surface was coated with a very thin layer of colloidal liquid silver (Ted Pella Inc.). Colloidal liquid silver was applied to the bottom side of the freshly peeled mica surface that did not contain the sample and was left to air dry for few minutes. A patch of colloidal liquid silver was applied to the center of a glass slide, forming a thin layer of silver, approximately the size of the mica substrate. To ensure proper grounding, a streak of silver coating leading from this central patch was added and extended to the opposite side of the glass slide. Silver-coated mica (with silver side down) was placed onto the wet silver patch on the glass slide. A function generator (Sanford Research System, model DS335) and lock-in-amplifier (Sanford Research System, model SR844 RF) were used to generate the AC and DC biases and monitor changes in vibration amplitude ( $A\omega^2$ ) and phase as a function of sample positions. Although the AC and DC biases are applied to AFM tips, the mica substrate is grounded. To optimize DREEM signals, AC and DC biases were adjusted from 0 to 20 and  $-1.5$  to 1.5 V, respectively.

**SV-AUC**—SV-AUC was carried out using 400  $\mu$ l of sample loaded into two-sector Epon centerpieces in an An60 Ti rotor in a Beckman Optima XL-I analytical ultracentrifuge, and run at 20 °C. Measurement was completed in intensity mode. Samples were run at 45,000 rpm and measured at 260 nm. For  $\bar{\nu}$  determination, three preparations of sample were run as above, with 0, 30, or 60% H<sub>2</sub><sup>18</sup>O (obtained from Cambridge Isotope Laboratories, Andover, MA) added in place of H<sub>2</sub><sup>16</sup>O. The obtained S values were then plotted as a function of solvent densities, linear regression was performed, and the  $\bar{\nu}$  was calculated by dividing the slope of the resulting line by the y intercept (see Fig. 3C). Linear regression was performed using GraphPad Prism software.

**2DSA/GA-MC**—All SV-AUC data were analyzed using UltraScan3 software, version 2.1 and release 1706, and fitting procedures were completed on XSEDE clusters at the Texas Advanced Computing Center (Lonestar, Stampede) and at the San Diego Supercomputing Center (Trestles) through the UltraScan Science Gateway. Raw intensity data were converted to pseudo-absorbance by using the intensity of the air above the meniscus as a reference and edited. Next, 2DSA was performed to subtract time-invariant noise and the meniscus was fit using 10 points in a 0.05-cm range. Arrays were fit using an S range of 1–20 S, an  $f/f_0$  range of 1–4 with 100 grid points for each, 10 uniform grid repetitions, and 400 simulation points. 2DSA was then repeated at the determined meniscus to fit radially invariant and time-invariant noise together using 5 iterations. von Holde-Weischet analysis was completed using these noise subtraction profiles to determine S. Where indicated, GA was ini-

## Characterization of ssDNA-Histone Complexes

tialized by binning major solutes in the 2DSA dataset, and run via LIMS. Major solutes from GA analysis were then binned and run again using GA with 50 MC iterations.

**Histone Octamer Transfer Assay**—To monitor histone octamer exchange between DNA strands, 200-bp double-stranded and 200-nt single-stranded reconstituted donor mononucleosomes were incubated at increasing concentrations (0, 0.5, 1, 2.5, 5, 25, and 50 nM) with the indicated radiolabeled naked acceptor DNA (25 nM). To determine DNA end requirement, histone octamer transfer was monitored in reactions with radiolabeled 200-nt single-stranded mononucleosomes (5 nM) and naked circular or linearized plasmid acceptor DNA at increasing concentrations (0, 1, 5, 10, 50, and 100 nM). Histone octamer transfer assays were performed in 10- $\mu$ l reactions (2 mM Hepes pH 7.5, 100 mM NaCl, 0.5 mg/ml of BSA, 1 mM DTT, 0.05% Tween) at room temperature (water bath) for 60 min. Glycerol was then added to a final 5% and samples were placed on ice and then separated on a 4% 0.5 $\times$  TBE PAGE pre-chilled to 4 °C. Gels were dried and analyzed by phosphorimaging or X-ray film exposure.

**Biotin-Streptavidin Pulldown**—To assess histone composition of ssDNA- and dsDNA-histone complexes, 200-bp double-stranded and 200-nt single-stranded reconstituted biotinylated chromatin was magnetically precipitated and electrophoretically separated in a 18% Tricine-SDS-PAGE. Biotinylated single-stranded DNA was custom ordered from Integrated DNA Technologies (IDT). Reconstituted chromatin samples (1  $\mu$ g) were incubated with 20  $\mu$ l of prewashed magnetic beads (10 mM Tris-HCl, pH 7.4, 0.25 mM EDTA, 50 mM NaCl) for 15 min at room temperature with agitation. After magnetic precipitation, supernatant was removed and equal amounts of 2 $\times$  SDS loading dye was added. Beads were resuspended in 1 $\times$  SDS loading dye, and samples were heated to 100 °C for 5 min before loading. Gels were subsequently visualized with standard Coomassie protein staining protocols.

**Chromatin Heat Stability Assay**—Reconstituted 200-bp double-stranded and 200-nt single-stranded mononucleosomes (50 nM) were incubated at the indicated temperatures for 30 min in 10  $\mu$ l (2 mM Hepes, pH 7.5, 70 mM NaCl, 0.2 mg/ml of BSA, 1 mM DTT, 0.05% Tween, 3 mM MgCl<sub>2</sub>). Glycerol (5%) and salmon sperm DNA (5  $\mu$ g) were added and samples were placed on ice before loading on a 4% 0.5 $\times$  TBE PAGE with ethidium bromide staining.

**Electrophoretic Mobility Shift Assay**—Assays were performed in 10- $\mu$ l reactions (20 mM Tris-HCl, pH 7.4, 5 mM DTT, 70 mM NaCl, 0.25 mg/ml of BSA, 20% glycerol) with 5 nM indicated chromatin substrate and increasing concentrations of RSC (0, 0.5, 1, 5, 10, 20, and 30 nM) and Fun30 (0, 1, 5, 10, 20, 30, and 60 nM) incubated on ice for 10 min. Samples were then electrophoretically separated on 4% 0.5 $\times$  TBE PAGE (79:1 acrylamide:bisacrylamide). Gels were dried and analyzed by phosphorimaging.

**Chromatin Remodeling Enzyme Kinetics**—ATPase rates of RSC and Fun30 were measured with saturated levels of DNA cofactor (1  $\mu$ g of plasmid) to estimate enzyme concentrations as previously described (37). Rates of ATP hydrolysis by RSC and Fun30 (10 nM each) were determined from the ratio of

cleaved <sup>32</sup>P to intact [ $\gamma$ -<sup>32</sup>P]dATP with the indicated substrate concentrations at 0, 10, and 20 min in 10- $\mu$ l reactions (20 mM Tris-HCl, pH 8.0, 0.2 mM DTT, 5% glycerol, 0.1% Tween, 35 mM NaCl, 5 mM MgCl<sub>2</sub>, 0.1 mg/ml of BSA). Reactions were stopped by pipetting 0.5  $\mu$ l onto chromatography paper (PEI-cellulose) and allowed to dry thoroughly with separation by capillary action in a chromatography chamber with a monobasic potassium phosphate solution, pH 3.5. Plates were air-dried and analyzed by phosphorimaging.  $K_m$  was calculated with GraphPad Prism software.

**Author Contributions**—N. L. A. performed the experiments displayed in Figs. 1, 2, 6, and 7. N. L. A. also performed all nucleosome reconstitutions. S. G. S. performed all analytical ultracentrifuge studies shown in Fig. 3; S. A. G. performed the electron microscopy studies (Fig. 4A); H. N. and P. S. provided resection enzymes; and P. K. and H. W. performed and supervised AFM/DREEM imaging (Figs. 4, B and C, and 5). All authors were involved in data analysis and manuscript preparation.

## References

1. Khanna, K. K., and Jackson, S. P. (2001) DNA double-strand breaks: signaling, repair and the cancer connection. *Nat. Genet.* **27**, 247–254
2. Ciccio, A., and Elledge, S. J. (2010) The DNA damage response: making it safe to play with knives. *Mol. Cell* **40**, 179–204
3. Papamichos-Chronakis, M., and Peterson, C. L. (2013) Chromatin and the genome integrity network. *Nat. Rev. Genet.* **14**, 62–75
4. Pâques, F., and Haber, J. E. (1999) Multiple pathways of recombination induced by double-strand breaks in *Saccharomyces cerevisiae*. *Microbiol. Mol. Biol. Rev.* **63**, 349–404
5. Niu, H., Chung, W.-H., Zhu, Z., Kwon, Y., Zhao, W., Chi, P., Prakash, R., Seong, C., Liu, D., Lu, L., Ira, G., and Sung, P. (2010) Mechanism of the ATP-dependent DNA end-resection machinery from *Saccharomyces cerevisiae*. *Nature* **467**, 108–111
6. Zhu, Z., Chung, W.-H., Shim, E. Y., Lee, S. E., and Ira, G. (2008) Sgs1 helicase and two nucleases Dna2 and Exo1 resect DNA double-strand break ends. *Cell* **134**, 981–994
7. Mimitou, E. P., and Symington, L. S. (2008) Sae2, Exo1 and Sgs1 collaborate in DNA double-strand break processing. *Nature* **455**, 770–774
8. Chu, W. K., and Hickson, I. D. (2009) RecQ helicases: multifunctional genome caretakers. *Nat. Rev. Cancer* **9**, 644–654
9. Chai, B., Huang, J., Cairns, B. R., and Laurent, B. C. (2005) Distinct roles for the RSC and Swi/Snf ATP-dependent chromatin remodelers in DNA double-strand break repair. *Genes Dev.* **19**, 1656–1661
10. Tsukuda, T., Fleming, A. B., Nickoloff, J. A., and Osley, M. A. (2005) Chromatin remodeling at a DNA double-strand break site in *Saccharomyces cerevisiae*. *Nature* **438**, 379–383
11. Bennett, G., Papamichos-Chronakis, M., and Peterson, C. L. (2013) DNA repair choice defines a common pathway for recruitment of chromatin regulators. *Nat. Commun.* **4**, 2084
12. Bennett, G., and Peterson, C. L. (2015) SWI/SNF recruitment to a DNA double-strand break by the NuA4 and Gcn5 histone acetyltransferases. *DNA Repair* **30**, 38–45
13. van Attikum, H., Fritsch, O., and Gasser, S. M. (2007) Distinct roles for SWR1 and INO80 chromatin remodeling complexes at chromosomal double-strand breaks. *EMBO J.* **26**, 4113–4125
14. van Attikum, H., Fritsch, O., Hohn, B., and Gasser, S. M. (2004) Recruitment of the INO80 complex by H2A phosphorylation links ATP-dependent chromatin remodeling with DNA double-strand break repair. *Cell* **119**, 777–788
15. Shim, E. Y., Hong, S. J., Oum, J.-H., Yanez, Y., Zhang, Y., and Lee, S. E. (2007) RSC mobilizes nucleosomes to improve accessibility of repair machinery to the damaged chromatin. *Mol. Cell Biol.* **27**, 1602–1613

16. Shroff, R., Arbel-Eden, A., Pilch, D., Ira, G., Bonner, W. M., Petrini, J. H., Haber, J. E., and Lichten, M. (2004) Distribution and dynamics of chromatin modification induced by a defined DNA double-strand break. *Curr. Biol.* **14**, 1703–1711
17. Chen, C.-C., Carson, J. J., Feser, J., Tamburini, B., Zabaronic, S., Linger, J., and Tyler, J. K. (2008) Acetylated lysine 56 on histone H3 drives chromatin assembly after repair and signals for the completion of repair. *Cell* **134**, 231–243
18. Chen, X., Cui, D., Papusha, A., Zhang, X., Chu, C.-D., Tang, J., Chen, K., Pan, X., and Ira, G. (2012) The Fun30 nucleosome remodeler promotes resection of DNA double-strand break ends. *Nature* **489**, 576–580
19. Adkins, N. L., Niu, H., Sung, P., and Peterson, C. L. (2013) Nucleosome dynamics regulates DNA processing. *Nat. Struct. Mol. Biol.* **20**, 836–842
20. Brookes, E., Cao, W., and Demeler, B. (2010) A two-dimensional spectrum analysis for sedimentation velocity experiments of mixtures with heterogeneity in molecular weight and shape. *Eur. Biophys. J.* **39**, 405–414
21. Demeler, B., Brookes, E., Wang, R., Schirf, V., and Kim, C. A. (2010) Characterization of reversible associations by sedimentation velocity with UltraScan. *Macromol. Biosci.* **10**, 775–782
22. Swygert, S. G., Manning, B. J., Senapati, S., Kaur, P., Lindsay, S., Demeler, B., and Peterson, C. L. (2014) Solution-state conformation and stoichiometry of yeast Sir3 heterochromatin fibres. *Nat. Commun.* **5**, 4751
23. Dalal, Y., Wang, H., Lindsay, S., and Henikoff, S. (2007) Tetrameric structure of centromeric nucleosomes in interphase *Drosophila* cells. *PLoS Biol.* **5**, e218
24. Wang, H., Dalal, Y., Henikoff, S., and Lindsay, S. (2008) Single-epitope recognition imaging of native chromatin. *Epigenetics Chromatin* **1**, 10
25. Wu, D., Kaur, P., Li, Z. M., Bradford, K. C., Wang, H., and Erie, D. A. (2016) Visualizing the path of DNA through proteins using DREEM imaging. *Mol. Cell* **61**, 315–323
26. Kaur, P., Wu, D., Lin, J., Countryman, P., Bradford, K. C., Erie, D. A., Riehn, R., Opresko, P. L., and Wang, H. (2016) Enhanced electrostatic force microscopy reveals higher-order DNA looping mediated by the telomeric protein TRF2. *Sci. Rep.* **6**, 20513
27. Benarroch-Popivker, D., Pisano, S., Mendez-Bermudez, A., Lototska, L., Kaur, P., Bauwens, S., Djerbi, N., Latrick, C. M., Fraissier, V., Pei, B., Gay, A., Jaune, E., Foucher, K., Cherfils-Vicini, J., Aeby, E., *et al.* (2016) TRF2-mediated control of telomere DNA topology as a mechanism for chromosome-end protection. *Mol. Cell* **61**, 274–286
28. Costelloe, T., Louge, R., Tomimatsu, N., Mukherjee, B., Martini, E., Khadaroo, B., Dubois, K., Wiegant, W. W., Thierry, A., Burma, S., van Attikum, H., and Llorente, B. (2012) The yeast Fun30 and human SMARCAD1 chromatin remodellers promote DNA end resection. *Nature* **489**, 581–584
29. Eapen, V. V., Sugawara, N., Tsabar, M., Wu, W.-H., and Haber, J. E. (2012) The *Saccharomyces cerevisiae* chromatin remodeler Fun30 regulates DNA end resection and checkpoint deactivation. *Mol. Cell Biol.* **32**, 4727–4740
30. Palter, K. B., Foe, V. E., and Alberts, B. M. (1979) Evidence for the formation of nucleosome-like histone complexes on single-stranded DNA. *Cell* **18**, 451–467
31. Caffarelli, E., Leoni, L., and Savino, M. (1985) Folding of single-stranded DNA on the histone octamer. *FEBS Lett.* **181**, 69–73
32. Caffarelli, E., De Santis, P., Leoni, L., Savino, M., and Trotta, E. (1983) Interactions of the histone octamer with single-stranded DNA: sedimentation analysis and low-angle X-ray diffraction. *Biochim. Biophys. Acta.* **739**, 235–243
33. Celeste, A., Fernandez-Capetillo, O., Kruhlak, M. J., Pilch, D. R., Staudt, D. W., Lee, A., Bonner, R. F., Bonner, W. M., and Nussenzweig, A. (2003) Histone H2AX phosphorylation is dispensable for the initial recognition of DNA breaks. *Nat. Cell Biol.* **5**, 675–679
34. Polo, S. E., and Jackson, S. P. (2011) Dynamics of DNA damage response proteins at DNA breaks: a focus on protein modifications. *Genes Dev.* **25**, 409–433
35. Byun, T. S., Pacek, M., Yee, M.-C., Walter, J. C., and Cimprich, K. A. (2005) Functional uncoupling of MCM helicase and DNA polymerase activities activates the ATR-dependent checkpoint. *Genes Dev.* **19**, 1040–1052
36. Luger, K., Rechsteiner, T. J., and Richmond, T. J. (1999) Expression and purification of recombinant histones and nucleosome reconstitution. *Methods Mol. Biol.* **119**, 1–16
37. Smith, C. L., Horowitz-Scherer, R., Flanagan, J. F., Woodcock, C. L., and Peterson, C. L. (2003) Structural analysis of the yeast SWI/SNF chromatin remodeling complex. *Nat. Struct. Biol.* **10**, 141–145
38. Luger, K., Rechsteiner, T. J., and Richmond, T. J. (1999) Preparation of nucleosome core particle from recombinant histones. *Methods Enzymol.* **304**, 3–19

## **Nucleosome-like, Single-stranded DNA (ssDNA)-Histone Octamer Complexes and the Implication for DNA Double Strand Break Repair**

Nicholas L. Adkins, Sarah G. Swygert, Parminder Kaur, Hengyao Niu, Sergei A. Grigoryev, Patrick Sung, Hong Wang and Craig L. Peterson

*J. Biol. Chem.* 2017, 292:5271-5281.

doi: 10.1074/jbc.M117.776369 originally published online February 15, 2017

---

Access the most updated version of this article at doi: [10.1074/jbc.M117.776369](https://doi.org/10.1074/jbc.M117.776369)

### Alerts:

- [When this article is cited](#)
- [When a correction for this article is posted](#)

[Click here](#) to choose from all of JBC's e-mail alerts

This article cites 38 references, 7 of which can be accessed free at <http://www.jbc.org/content/292/13/5271.full.html#ref-list-1>